Magnetic, electronic, and thermal transport properties of Eu$_{0.55}$Sr$_{0.45}$MnO$_3$

J. Z. Wang, J. R. Sun,[*] G. J. Liu, Y. W. Xie, D. J. Wang, T. Y. Zhao, and B. G. Shen

Beijing National Laboratory for Condensed Matter Physics, Institute of Physics, Chinese Academy of Sciences,
Beijing 100080, People's Republic of China

X. G. Li

Structure Research Laboratory, Department of Material Science and Engineering, University of Science and Technology of China,
Hefei, Anhui 230026, People's Republic of China

Magnetic, electronic, and thermal transport properties of Eu$_{0.55}$Sr$_{0.45}$MnO$_3$ have been experimentally studied. The compound is found to exhibit a complex magnetic behavior with the change of temperature and magnetic field. Without magnetic field, it stays in a Griffiths-like state in a wide temperature range above ~100 K, characterized by the presence of ferromagnetic (FM) clusters of the size of ~8 Mn ions, and an antiferromagnetic (AFM) state below ~100 K, evidenced by thermopower and heat conductivity. FM phase emerges and grows in the AFM matrix with applied field, resulting in a series of phase transitions from the paramagnetic (PM) state first to the AFM state, then to the FM and the AFM states upon cooling (~0.8 T $< H < $ ~1 T), or a simple PM-FM transition ($H > $ ~2.3 T). The AFM state is unstable under high fields, and the high- and low-temperature AFM transitions are depressed by the fields above ~1 and ~2.3 T, respectively. The FM transition is incomplete when the field is below ~1.5 T, leading to a coexistence of the FM and PM (or AFM) phases in the intermediate temperature range. A spin-glass-like behavior is observed in the AFM background below ~50 K. Significant response of resistance, thermopower, and heat conduction to magnetic transition, either FM or AFM transition, has been observed. Unlike the typical AFM manganites, for which usually a depression of thermal conduction occurs at the AFM state, the AFM transition in Eu$_{0.55}$Sr$_{0.45}$MnO$_3$ enhances the thermal conduction. From the PM phase to the AFM phase and to the FM phase, thermal conductivity increases monotonically. A remarkable result of the present work is the different behaviors of thermopower and resistivity. The former displays a metallic behavior below a distinct temperature that is significantly lower than the metal-to-insulator transition temperature determined by resistivity. Furthermore, thermopower remains metallic while the resistivity shows up an upturn due to the AFM transition in the low-temperature range under the field of 1.5 T. Based on these data, a magnetic phase diagram is proposed.

PACS number(s): 75.47.Lx, 73.50.Lw, 74.25.Fy

I. INTRODUCTION

Colossal magnetoresistance (CMR) and the effects associated with spin, charge, and orbital degrees of freedom in perovskite manganites have received wide attention in recent years because of their rich physics and great potential in practical application.[1] It has been found that magnetic field can significantly affect the metal-to-insulator transition of the manganites, leading to the CMR effect.[2–4] In the meantime, spin, charge, and orbital orders experience a significant change. The coexistence and competition of double exchange (DE), which favors a ferromagnetic (FM) order, superexchange (SE), which supports an antiferromanetic (AFM) order, and Coulomb interactions, are believed to be responsible for the striking properties of the manganites. Any external stimulus that disturbs the unstable balance between the competitive mechanisms can result in dramatic effects.[5–7]

The strongest competition between different mechanisms may take place in Eu$_{1-x}$Sr$_x$MnO$_3$ ($0.42 \leq x \leq 0.5$). As previously reported,[8–10] the ground state of Eu$_{1-x}$Sr$_x$MnO$_3$ is AFM at low temperatures because of the depression of the DE interaction by the presence of smaller Eu^{3+} ions. However, the FM and AFM competition is so strong that a small field can effectively stabilize the FM order. Under an appropriate magnetic field, the compound experiences a paramagnetic

(PM) to FM transition and a FM to AFM transition in sequence with the decrease of temperature. Although these behaviors are similar to those of other manganese oxides such as Nd$_{0.5}$Sr$_{0.5}$MnO$_3$ and Pr$_{0.5}$Sr$_{0.5}$MnO$_3$, the high field sensitivity is absent in the latter compounds. There is further evidence for the particularity of Eu$_{1-x}$Sr$_x$MnO$_3$. It has been argued that there is no stable charge ordering even in half-doped Eu$_{0.5}$Sr$_{0.5}$MnO$_3$.[9,11] Different from most of the half-doped manganites, a recent study revealed a significant decrease of heat capacity when the compound evolves from the AFM to the FM state.[12] All these results indicate that Eu$_{1-x}$Sr$_x$MnO$_3$ deserves special attention. It provides us an alternative opportunity for a thorough exploration of the underlying physics of the CMR and related effects in the manganites.

There are a number of studies on Eu$_{1-x}$Sr$_x$MnO$_3$; however, most of the previous work concentrated on the magnetic and resistive behaviors. In contrast, heat transport and thermoelectric properties of Eu$_{1-x}$Sr$_x$MnO$_3$ have scarcely been concerned. As is well known, heat conduction is a property associated with the lattice dynamics of the compound, while thermopower is a measurement of the effect of charge accumulation produced by the temperature gradient.[13–15] A combined investigation on magnetic, electronic, and thermal properties can provide a stereo description for the complex phase transition in Eu$_{1-x}$Sr$_x$MnO$_3$, which is expected to be

helpful for uncovering the hidden aspects of $Eu_{1-x}Sr_xMnO_3$, therefore for a comprehensive understanding of the distinctive properties of the manganites. Based on these considerations, in this paper, we performed a systematic study on $Eu_{0.55}Sr_{0.45}MnO_3$ (ESMO), a compound particularly sensitive to external field, with the use of various techniques. Special attention has been paid to the effects of field-induced phase transitions. A significant response of thermopower and heat conduction to magnetic transition, either FM or AFM, was detected, which results in some unexpected behaviors.

II. EXPERIMENT

The polycrystalline sample ESMO was prepared by the conventional solid-state reaction method. Well mixed stoichiometric amounts of the Eu_2O_3, $SrCO_3$, and $MnCO_3$ powders were calcined first at 1000 °C for 24 h, then at 1250 °C for 48 h, with an intermediate grinding for homogenization. The resultant product was ground, pelletized, and sintered at 1350 °C for another 36 h, then furnace cooled to room temperature.

Phase purity and crystal structure of the sample were studied by powder x-ray diffraction performed by a Rigaku x-ray diffractometer with a rotating anode and Cu $K\alpha$ radiation. A Quantum Design superconducting quantum interference device magnetometer (MPMS-7) was used for the magnetic measurements. Resistance, heat conduction, and thermopower were determined simultaneously by a Physical Property Measurement System (PPMS-14H). A Matec-7700 series equipment (Matec Instrument Companies, USA) was used for the measurement of ultrasonic sound velocity and attenuation. All the data presented here were collected in the warming process after cooling the sample to the predetermined temperatures without magnetic field.

III. RESULTS

A. Crystal structure

As revealed by the Rietveld analysis of the powder x-ray diffraction spectrum collected at room temperature, the sample is single phase of orthorhombic structure (space group $Pbnm$) with the lattice parameters of $a=0.5426$ nm, $b=0.5427$ nm, and $c=0.7653$ nm. The unit-cell volume is 0.225 nm^3, ~1% smaller than that of $Pr_{0.5}Sr_{0.5}MnO_3$.[16] This is obviously the consequence of the presence of smaller Eu^{3+} ions (compared with Pr^{3+}) and is expected to have a strong impact on the magnetic and resistive properties of ESMO.

B. Magnetism

Figure 1 shows the temperature-dependent magnetization measured under selected fields between 0.1 and 5 T (top panel). The compound exhibits rich, yet field-sensitive, magnetic behaviors. It stays in an AFM state below ~100 K without magnetic field, as evidenced by the thermopower and heat conductivity data presented in the following sections. FM phase emerges and grows in the AFM matrix with applied field, resulting in a series of phase transitions from the PM state first to the AFM state, then to the FM and the
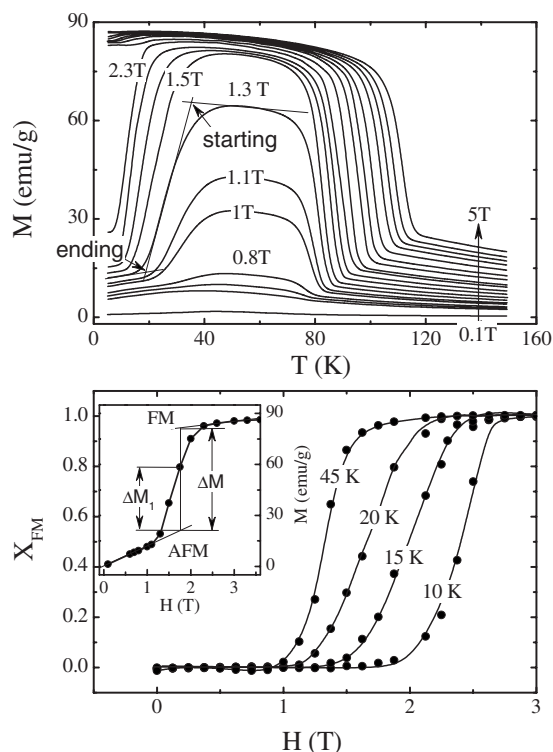

FIG. 1. Top panel: temperature-dependent magnetization measured under selective fields between 0.1 and 5 T. Straight lines mark the definition of phase transition temperature. Bottom panel: volume fraction of the FM phase as a function of magnetic field at the temperatures of 10, 15, 20, and 45 K. The inset plot in the bottom panel shows the magnetization curve corresponding to $T = 20$ K. Solid lines are guides for the eyes.

AFM states upon cooling (~0.8 T $< H < $ ~1 T), or a simple PM-FM transition ($H \sim 2.3$ T). Magnetic field drives the Curie temperature to high temperatures at a rate of ~8.3 K/T, significantly expanding the temperature span of the FM phase. In contrast, the AFM phase becomes unstable under magnetic field, and the high- and low-temperature AFM transitions are depressed by the fields above 1 T (see the following section) and 2.3 T, respectively. These results are similar to those previously reported for the compound $Eu_{0.58}Sr_{0.42}MnO_3$.[8,10] A careful analysis indicates that the FM transition is incomplete when the field is below ~1.5 T, leading to a coexistence of the FM and the PM (or AFM) phases in a wide temperature range. The bottom panel of Fig. 1 gives the proportion of the FM phase (X_{FM}) as a function of applied field, defined by the ratio of the detected magnetization (ΔM_1) to that expected (ΔM) when the compound is completely in the FM state (inset in Fig. 1). Taking the result obtained at $T=20$ K as an example, the specimen is AFM under low magnetic fields, FM phase emerges and develops when the applied field exceeds ~1.2 T, and the AFM phase is completely converted into the FM phase above the field of ~2.3 T. It is possible that the presence of small Eu^{3+} ions leads to an enhanced distortion of the MnO_6 octahedron, thus a significant depression of the DE process. However, the competition between the DE and SE interactions is so strong that a small external field can effectively disturb their unstable balance.
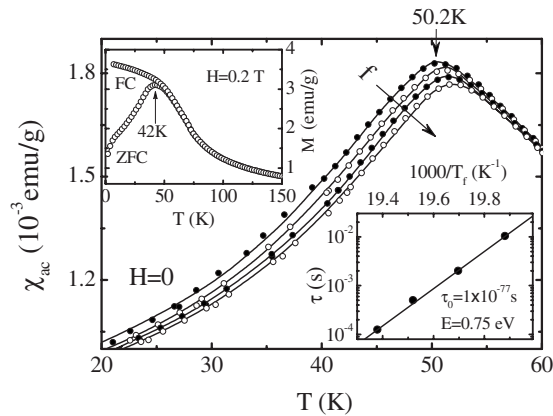
FIG. 2. Susceptibility measured under the ac field of 10 Oe and the frequency from 47 to 7997 Hz. Arrow in the figure marks the shift of the curve with frequency. Solid lines are guide for the eyes. The top inset displays the magnetization curves obtained under the dc field of 0.2 T. FC, field cooling; ZFC, zero field cooling. Bottom inset is a plot showing relaxation time as a function of reciprocal T_f, the temperature of the susceptibility peak.

The low-temperature AFM transition of ESMO may be inherited from $EuMnO_3$, for which an AFM transition takes place at ~ 55 K,[9,17] and can be depressed completely by a field above 2.3 T. However, the magnetic behaviors of ESMO are much more complex compared with $EuMnO_3$ because of the introduction of divalent ions Sr^{2+}. As shown in Fig. 2, the ac susceptibility exhibits a sharp peak of frequency dependence, shifting from ~ 50.2 to ~ 51.6 K as the frequency increases from 47 to 7997 Hz. A splitting of the magnetization curves respectively recorded in the zero-field-cooling and field-cooling processes, together with a low-temperature shift of susceptibility peak with applied field, is observed (top inset in Fig. 2). These results suggest the spin-glass-like nature of the compound. Based on the Néel-Arrhenius law $\tau = \tau_0 \exp(E/k_B T_f)$, the spin-glass-like behavior can be quantitatively analyzed, where $\tau = 1/f$ (frequency of the ac measurements), τ_0 is the gyromagnetic precession time, E the activation energy for the relaxation, and T_f the peak temperature of the susceptibility. It is believed that τ_0 is usually $\sim 10^{-200}$ s and $E = 0.8$–24 meV for typical spin glass and $\sim 10^{-10}$–10^{-13} s for superparamagnetism. A simple calculation gives $\tau_0 \sim 10^{-77}$ s and $E \approx 750$ meV for the present sample (bottom inset in Fig. 2). The relaxation in ESMO is much slower than that in a spin glass system. These results indicate that the low-temperature ground state of ESMO may be a cluster-glass state rather than a spin glass state.[18,19] Although the uncertainty of T_f affects considerably the accuracy of τ_0 and E because of the small shift of T_f with frequency, the general tendency is unambiguous. It should be emphasized that the spin-glass-like behavior in ESMO takes place in an AFM background, instead of a PM matrix as usually happened. The reason for this may be the formation of FM clusters due to the presence of Sr^{2+} ions, which leads to a frustration of the long range AFM order.

To give a definite answer to whether FM clusters exist in the AFM matrix may require the data of neutron scattering. However, a simple analysis on susceptibility does suggest the
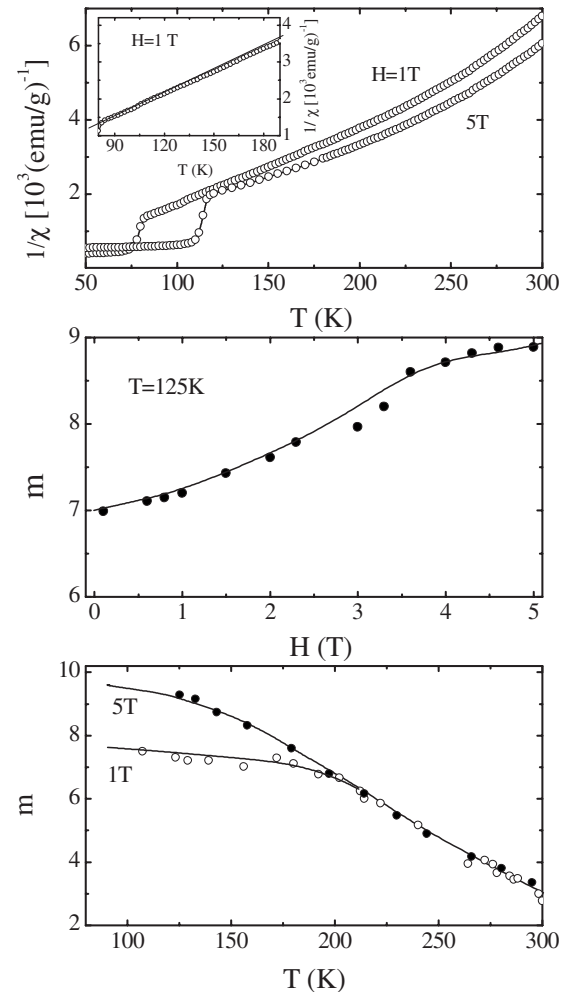

FIG. 3. Top panel: reciprocal susceptibility as a function of temperature obtained under the fields of 1 and 5 T. Middle panel: sizes of the FM clusters as functions of magnetic field obtained at a fixed temperature of 125 K. Bottom panel: sizes of the FM clusters as functions of temperature. The inset plot is a close view of reciprocal susceptibility near the Curie temperature. Solid lines are guides for the eyes.

presence of obvious short-range magnetic order in the PM phase. In general, the information on the magnetic entities can be obtained from the analysis of the susceptibility above the Curie temperature. It is easy to derive that the Curie-Weiss law will be $\chi = Nm(T,H)g^2S^2\mu_B^2/3k_B(T-T_\theta)$ ($mS \gg 1$) if the FM clusters of the average size of m Mn ions exist,[20] where N is the number of Mn ions in 1 g ESMO, $g=2$ (Landé factor), S the quantum number of spins, T_θ the PM Curie temperature, and k_B the Boltzmann constant. It is found that the susceptibility of ESMO obtained under the field of 1 T can be excellently fitted by the modified Curie-Weiss law using the parameters $T_\theta \approx 18.4$ K and $m \approx 7.2$ (top panel of Fig. 3) if the magnetic moment of the Mn ion is set to $gS\mu_B = 3.55\ \mu_B$ (the weighted average of Mn^{3+} and Mn^{4+}). It can be a consequence of strong magnetic correlation that binds adjacent spins together and results in a significant local magnetic order. This result reveals the presence of the FM clusters composed of ~ 8 Mn ions in the PM phase.
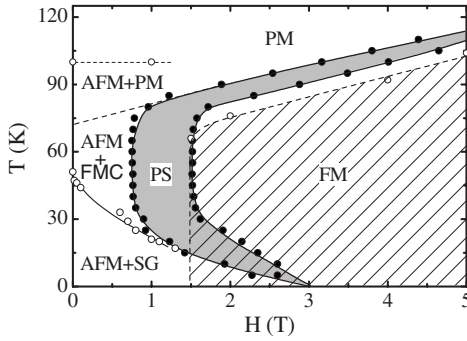
FIG. 4. Phase diagram of ESMO depicted in the *H-T* plane. Gray area marks the region where two phases coexist and hatched area marks the region where metallic conduction prevails. PS, phase separation; SG, spin-glass-like phase; AFM+FMC, AFM matrix +FM clusters.

FIG. 5. Temperature-dependent resistivity of ESMO measured under different magnetic fields.

Similar results are obtained by Wang *et al.* for $(Sm,Nd)_{0.55}(Ca,Sr)_{0.45}MnO_3$.[19]

As a supplement, we would like to emphasize that the magnetic cluster is merely an equivalent description of short-range magnetic order. It is obvious that the stronger the short-range order is, the larger the cluster size will be.

Effects of magnetic field are not strong, and a slight growth of the FM cluster is observed as the field rises (middle panel of Fig. 3). In contrast, increase in temperature causes considerable decomposition of the FM cluster. This effect is weak when the temperature is low but strong above 190 K. Cluster size decreases from ~9 for $T=120$ K to ~3 for $T=300$ K under a constant field of 5 T (bottom panel of Fig. 3). However, the cluster size is obviously larger than that observed in other manganites such as $La_{0.7}Ca_{0.3}MnO_3$, for which generally two Mn ions group together.[21]

Presence of a Griffiths-like state, characterized by the co-existence of FM clusters and PM phase well above the Curie temperature, has recently been proved to be a general feature of the manganites.[22] For ESMO, the contributions to susceptibility may mainly come from magnetic clusters considering the fact that the variation of the Curie-Weiss constant is small as the applied field increases from ~0 to 5 T.

Figure 4 is a magnetic phase diagram of ESMO obtained by summarizing the data in Figs. 1–3. Edges of the gray area are determined by the starting/ending temperature of the phase transition. The hatched area marks the metallic phase suggested by thermopower (see the following sections). Appearance of spin-glass-like behavior and deviation of magnetization data from the Curie-Weiss law in the temperature range from ~50 to 75 K (top inset in Fig. 2) suggest the presence of FM clusters (FMC) in the AFM matrix.

C. Resistive and thermoelectric properties

A typical feature of the manganite is the strong magnetic-resistive interplay. Figure 5 presents the temperature-dependent resistivity measured under selected magnetic fields between 0 and 5 T. As expected, the sample exhibits an insulating behavior without magnetic field with an unobvious anomaly at ~100 K (see the context). In response to
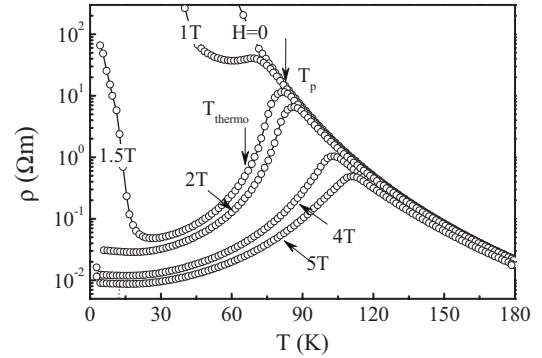
the field-induced FM ordering, a tendency to metallic conduction appears. A visible, however, incomplete, resistive transition can be identified from the $\rho(T)$ curve under the field of 1 T. As the population of the FM phase grows further under a higher field of $H=1.5$ T, an insulator-to-metal transition occurs at $T_p \approx 82$ K in accordance with the magnetic one, resulting in a resistivity drop by 3 orders of magnitude. These behaviors and the abrupt resistive upturn below ~20 K due to the AFM transition vividly demonstrate the magnetic-resistive interplay in ESMO. Further increase in magnetic field drives the resistive transition to high temperatures without affecting the general $\rho(T)$ relation except for the reduction of the residual resistivity.

A careful analysis indicates the presence of an excellent $\ln \rho \propto (T_0/T)^{1/2}$ relation in the high-temperature range in ESMO (Fig. 6). This process occurs under all of the magnetic fields concerned, with only a slight decrease of T_0 against H ($T_0^{1/2} \sim 192.3$ $K^{1/2}$ for $H=0$ and ~184.4 $K^{1/2}$ for $H=5$ T), though the temperature for the resistive transition increases significantly. There are two possible mechanisms for this kind of transport behavior. The first one is the variable-range hopping of electrons with a considerable interelectron interaction, and the second one is the charge hopping between conducting clusters embedded in an insulating matrix. The former is a process that takes place in a homogeneous system, whereas the latter takes place in an inhomogeneous system. It is generally believed that the transport behavior of the manganite is dominated by the former. However, whether the inhomogeneous magnetic structure of ESMO can add something new is also an interesting issue.

An obvious deviation of the resistivity from the $(T_0/T)^{1/2}$ law is detected below 100 K, which is indicative of a different mechanism for the electron conduction in the AFM state (top inset in Fig. 6). It is possible that the AFM ordering influences the electron-lattice coupling, resulting in the visible anomaly of transport behavior.

The magnetic transition in ESMO is first order in nature, noting the modifiability of the Curie temperature by magnetic field. There are two possible processes for the phase transition with the decrease of temperature. The first one is the growth of the FM phase, occurring in a rather narrow temperature region below T_p, as marked by the gray area in Fig. 4, and the second one is the alignment of the spins
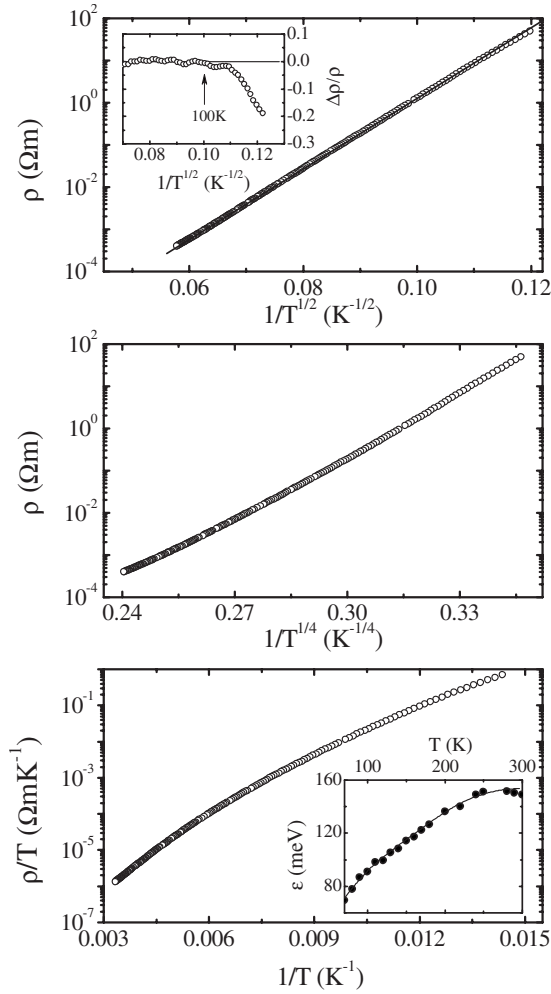
FIG. 6. Comparison of the conduction processes in ESMO without external field. Variable-range hopping with electron correlation (top panel), variable-range hopping without electron correlation (middle panel), and adiabatic small polaron hopping (bottom panel). The top inset shows the deviation of the resistivity from the $1/T^{1/2}$ law below ~ 100 K. The bottom inset displays the activation energy as a function of temperature in the picture of small polaron hopping. Solid line is a guide for the eyes.

FIG. 7. Top and middle panels: temperature dependence of the thermopower of ESMO measured under selected magnetic fields. T_{thermo}, defined by the rigid corner of the curve, marks the temperature below which metallic conduction prevails. The top inset shows the thermopower versus reciprocal temperature obtained without external field. Bottom panel: the critical temperature for the resistive transition seen by resistivity (T_p) and the temperature for metallic conduction defined by thermopower (T_{thermo}). The bottom inset is a comparison of the $\rho(T)$ and $S(T)$ relations.

within the FM domains, the process approaching saturation. However, discrimination of these two processes is not clear in the resistive data. The resistivity reduces smoothly in a wide temperature range below T_p ($\approx T_c$). To get a deep understanding of the phase transition, the thermoelectric property of ESMO was further studied. A remarkable result is the sensitivity of thermopower $S(T)$ to phase transition, either the AFM or the FM phase transition. As shown in Fig. 7, without external field, two clear thermopower peaks appear, corresponding to the AFM transitions at ~ 50 and ~ 100 K. The intermediate thermopower peak at ~ 70 K in the case of $H=1$ T is a response to the incomplete FM transition (see Fig. 4). With the increase of magnetic field, the thermopower becomes negative in the whole temperature range concerned, which signifies the electron character of the charge carrier in ESMO, and the $S(T)$ relation also undergoes a considerable change (Fig. 7). There is a definite temperature (T_{thermo}) that
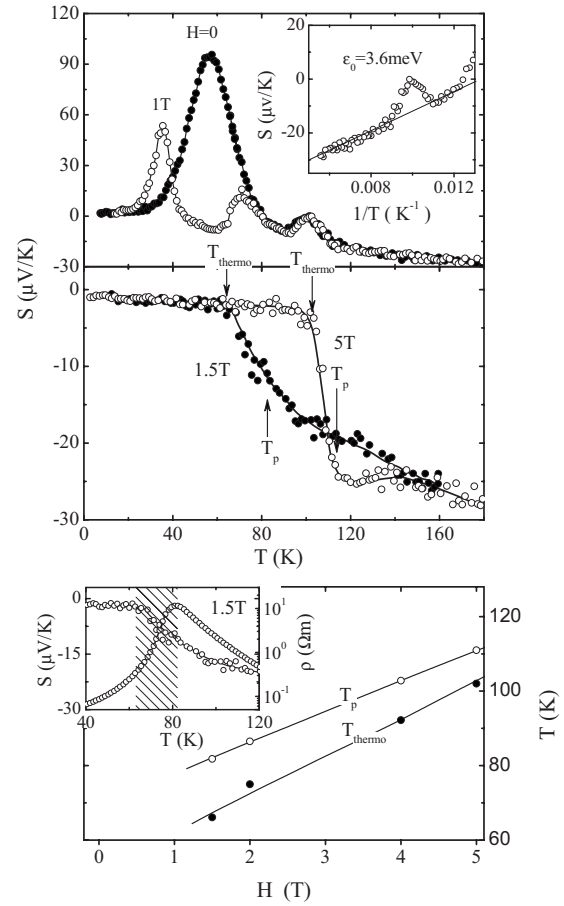
divides the $S(T)$ curve into a linear and a nonlinear part when the magnetic field exceeds 1.5 T. The excellent linear relation below T_{thermo}, which is scarcely observed before in the manganite, is believed to be a signature of metallic conduction. Magnetic field significantly affects T_{thermo}, driving it from ~ 66 K for $H=1.5$ T up to ~ 103 K for $H=5$ T. In contrast, the value of $S(T)$ is essentially independent of the magnetic field below T_{thermo}, though the resistivity varies by orders of magnitude (Fig. 5). The most interesting observation is the obvious discrepancy of T_p with T_{thermo}, both of which signify the occurrence of metallic conduction. The largest difference appears under the field of 1.5 T, where T_p is ~ 82 K, whereas T_{thermo} is ~ 66 K. The temperature difference changes with the applied field, decreasing from ~ 16 K for $H=1.5$ T to ~ 9 K for $H=5$ T (bottom panel of Fig. 7). This result indicates that, although the resistive transition sets in at T_p, a real metallic conduction is not established until the sample is cooled below T_{thermo}. In the temperature range between T_{thermo} and T_p, the value of thermopower dis-
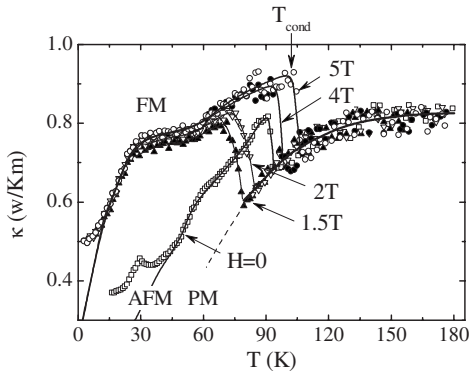
FIG. 8. Temperature dependence of thermal conductivity of ESMO measured under selected fields. T_{cond} marks the transition to a high thermal conductivity state. Solid and dashed lines are guides for the eyes.

plays a rapid decrease with the increase of temperature, especially under the fields of 4 and 5 T.

Based on the free electron approximation, the metallic thermopower has the form of $S=-(\pi/6e)^2(k_B^2 T/E_F)$.[23] The Fermi energy can be derived from the slope of the $S(T)$ curve, and it is $E_F \approx 0.7$ eV. Using the simplistic approximation of the parabolic band and the spherical Fermi surface, $E_F=(3n\pi^2)^{2/3}\hbar^2/2m^*$, the effective electron mass turns out to be $m^*/m_0 \approx 3$, where m_0 is the free electron mass and $n=9.8\times10^{21}/cm^3$ has been adopted for the calculation. The large electron mass reveals that the conduction band is rather narrow even in the metallic state.

In the temperature range above 110 K, the thermopower can be well described by the formula $S=k_B/e\ (\varepsilon_0/k_B T+\alpha)$, where ε_0 is the energy difference between identical lattice distortions with and without the hole, for polaron conduction, or between the conduction band and the Fermi level for a semiconductor.[15,24] A simple analysis indicates that ε_0 is low, ~ 3.6 meV above ~ 110 K (top inset in Fig. 7), much smaller than that expected for an ordinary semiconductor ($\sim 0.1 - \sim 1$ eV), and the same order in magnitude as that of the generation energy of a polaron. Approximating the resistivity above T_p by $\rho \propto T\exp(\varepsilon/k_B T)$, it is easy to obtain that the activation energy ε for the conduction is of the order of 10^2 meV in magnitude. The great difference between ε_0 and ε reveals the polaronic character of the charge transport process in ESMO. In the high-temperature limit, the deduced thermopower is -48 μV/K. Setting x to 0.45 and β to 2, we obtained $\alpha=-k_B/e\ \ln[\beta x/(1-x)]\approx-44$ μV/K, which is a value in good agreement with that experimentally observed, where β represents the spin degeneracy and x the hole concentration in the compound.[25]

D. Thermal conductive property

Heat conduction is a process associated with lattice dynamics of the materials. It includes contributions from phonons, electrons, and spin waves. Figure 8 shows the temperature dependence of the thermal conductivity of ESMO measured under various magnetic fields. The thermal conduction is low even at high temperatures, generally below

1 W/K m. With the decrease of temperature, it exhibits first a monotonic decrease, then an abrupt jump at exactly the same temperature where phase transition occurs, and finally a smooth reduction again. All the experimental data fall into essentially the same curve in the PM state, regardless of the magnetic field. Corresponding to the FM, AFM, and PM states, in contrast, three different tendencies appear in the low-temperature range. As shown by the thermoelectric data (Fig. 7), a field of 1.5 T destroys the AFM transition at ~ 100 K, which expands the PM phase down to ~ 80 K (Fig. 4). The similarity of the κ-T relations of the PM and AFM phases can be seen by comparing the thermal conductivity in the temperature interval from ~ 80 to ~ 94 K. In contrast, the thermal conduction of the FM phase exhibits a completely different temperature dependence. As shown in Fig. 8, in the temperature range between ~ 80 and ~ 94 K, the compound transits from the PM to the AFM and to the FM state as the applied field increases from 0 to 5 T. This allows a comparison of the thermal conductivity of the three magnetic states for a given temperature. It is obvious that from the PM phase to the AFM phase and to the FM phase, thermal conductivity increases monotonically.

There is evidence that the contribution from spin waves to heat conduction is fairly small, negligible compared to the lattice term at all but low temperatures. A rough estimate based on the formula $\Delta\kappa_m=\Delta C v_m^2 \tau_m/3$ shows that the thermal conductivity change produced by spin waves is ~ 0.05 W/K m under the modest magnetic field of 3 T, where ΔC denotes the variation of heat capacity at T_C and $v_m=600$ m/s and $\tau_m=2\times10^{-12}$ s are the velocity and lifetime of the long-wavelength spin waves, respectively.[10,26] Furthermore, the contribution from conduction electrons can be calculated based on Wiedmann-Franz's law $\kappa_e=LT/\rho$, and it is $3\times10^{-8}-2.5\times10^{-4}$ W/K m, where $L=2.45\times10^{-8}$ V^2/K^2 is Lorentz's constant for the free electron approximation.[27] It is extremely small because of the high resistivity of ESMO in the temperature range considered ($\rho > 10^{-2}$ Ω m).

Changes of thermal conductivity at the FM or AFM transition are the order of ~ 0.18 W/K m in magnitude (Fig. 8). Therefore, it can be ascribed to neither spin waves nor electrons. Enhancement of thermal conduction in the FM state has been observed before in other manganites and explained in terms of the depression of electron-phonon coupling.[26,28,29] As is well known, a distinctive feature of the manganite is the presence of strong Jahn-Teller effects, especially in the PM state. The static or dynamic Jahn-Teller distortions of the MnO$_6$ octahedra, distributed randomly in the lattice, will depress the thermal conduction by enhancing the phonon-phonon and electron-phonon scattering. The Jahn-Teller effects can be depressed by a FM ordering due to the improvement of charge transferring in the FM state. This in turn produces two effects. The first one is the weakening of the phonon-phonon and electron-phonon scattering, and the second one the enhancement of electron conduction. Both effects will favor thermal conduction. This explains the jump of the thermal conduction at the FM transition. To demonstrate the correspondence between different processes, in Fig. 9, we present the magnetization, resistivity, thermopower, and thermal conductivity as functions of applied
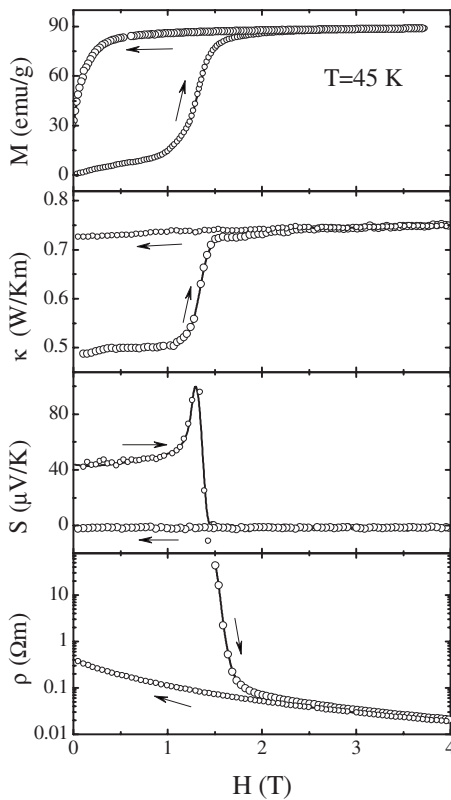
FIG. 9. Magnetization, resistivity, thermopower, and thermal conductivity as functions of magnetic field measured at a fixed temperature of $T=45$ K.
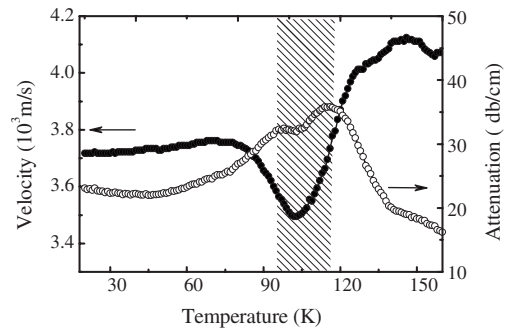

FIG. 10. Ultrasonic sound velocity and attenuation of ESMO as functions of temperature. Hatched area marks the structure transition.

while the decrease of heat conduction observed in other half-doped manganites could be attributed to the depression of electron conduction. It should be noted that the electron-phonon coupling associated with the Jahn-Teller effects remains in the AFM phase. Therefore, although the thermal conduction of the AFM phase is higher than that of the PM phase, it is still lower than that of the FM phase.

IV. DISCUSSION AND CONCLUSIONS

The AFM transition at ~100 K is not obvious from either the magnetic or the heat capacity data (not shown). The thermopower, heat conduction, sound velocity of the present work, and the evidence from the literature confirm the occurrence of this transition.[8,10] This is different from $Eu_{0.58}Sr_{0.42}MnO_3$, for which a thermal anomaly due to the AFM transition can be identified from the heat capacity curve.[10]

Magnetic data indicate the appearance of AFM phase in the low-temperature range (Fig. 4). The thermopower data confirm the occurrence of a phase transition around ~55 K without magnetic field, which may suggest the difference of the AFM phases separated by this transition. In analogy to $EuMnO_3$, which exhibits an A-type AFM phase below ~55 K, the low-temperature phase of ESMO may be an A-AFM structure. This phase transition downward shifts to ~36 K under the field of 1 T (Fig. 7). It is also consistent with the magnetic data. Figure 1 shows that the FM-AFM transition under the same field sets in at ~38 K and finishes at ~20 K. As for the high-temperature AFM phase, its magnetic structure is still unclear. It could be a CE-type AFM phase, which appears in a similar compound $Sm_{0.55}Sr_{0.45}MnO_3$.[32] It is obvious that a further study based on neutron diffraction is required to clarify the AFM structure of ESMO. The same notation has been used for the AFM phases in Fig. 4 because of the lack of knowledge about their exact magnetic structures.

It has been experimentally evidenced that the transport behavior of the manganite has a character of large polaron diffusion in the low-temperature range, while it has a small polaron hopping above T_P. The metallic transition is believed to be a continuous process, corresponding to a crossover from small to large polaron. The resistive and thermoelectric

field measured at a fixed temperature of $T=45$ K, where a strong magnetic field effect is expected. The system is AFM under low fields, and the FM phase appears when the magnetic field exceeds ~1 T. Thermopower and thermal conduction begin to increase at the exact field. $S(T)$ gets its peak value when ~40% FM phases appear. Thermal conduction takes the maximum value and thermopower takes the minimum value as magnetization reaches the saturation state.

Increase of thermal conduction in the AFM state has scarcely been observed before in the manganite. Quite the reverse, AFM ordering was found to disfavor heat conduction, as occurred in manganites such as $Pr_{0.5}Sr_{0.5}MnO_3$, $Nd_{0.5}Sr_{0.5}MnO_3$, and $Sm_{1-x}Ca_xMnO_3$.[26,28,30] The low-temperature crystal structure of ESMO is not studied because of the limit of the experimental condition. In analogy to $Sm_{0.5}Sr_{0.5}MnO_3$, which is a compound with similar magnetic properties to those of ESMO, the AFM transition at ~100 K could lead to an expansion of the unit cell along the a and b axes and a contraction along the c axis.[31] In fact, analysis of sound velocity of ESMO manifests a lattice softening as the AFM transition is approached, as happened to the manganites that experiences a charge ordering (Fig. 10). This result confirms the occurrence of a structure transformation at ~100 K. A direct consequence of this is the cooperative ordering of the Jahn-Teller-distorted MnO_6 octahedra to optimize elastic energy. As a result, effects due to randomly distributed Jahn-Teller distortions are ruled out. This may explain the enhancement of heat conduction at ~100 K,

data in Figs. 5 and 7 suggest the presence of two distinctive temperatures T_P and T_{thermo}. This result is reliable, considering the fact that the resistance and thermopower have been simultaneously determined by PPMS. A natural explanation is that the resistive transition sets in at T_P and ends at T_{thermo}. It is possible that the volume fraction of the FM phase exceeds the percolation threshold ($\sim$20%) at T_P, leading to the formation of metallic paths through the sample.

A direct calculation gives the normalized magnetization at $T_{thermo}(H)$, $\sim$88.8%, 87.6%, $\sim$88.4%, and $\sim$88.9%, corresponding to the fields of 1.5, 2, 4, and 5 T, respectively. Fluctuation of the data could be a consequence of experimental error because of the rapid magnetization change near the Curie temperature. This result implies that the "real" metallic conduction appears only when the compound approaches the state of magnetic saturation. This is different from resistivity, which defines a metallic conduction by the relation $d\rho/dT > 0$ that is satisfied when FM domains percolate. This result indicates that thermopower could give a clear definition for the lower bound of the temperature window of the resistive transition, which is usually unknown for the manganites. This result also reveals the different sensitivities of resistivity and thermopower to the different stages of phase transition. As a supplement, we would like to point out that not only thermopower but also heat conduction experiences a state switching between T_P and T_{cond} ($\approx T_{thermo}$) (Fig. 8).

The lowest magnetic field for metallic conduction is $\sim$1.5 T. This field is obviously not enough to stabilize the FM phase, as demonstrated by the entrance of the AFM state below $\sim$30 K (Fig. 1). The correspondence between magnetization and resistivity is obvious. The resistive upturn begins at $\sim$20 K, where the FM fraction is $\sim$29% (bottom panel of Fig. 1). This value is close to the threshold of site percolation of a cubic lattice. With the decrease of the FM population, resistivity increases rapidly. It is interesting to note the discrepancy of resistivity and thermopower in the low-temperature region under this field. With the decrease of temperature, the former exhibits an abrupt upturn while the latter remains metallic, without any responses to the former (Figs. 5 and 7). Metallic conduction preserves when magnetization drops from $\sim$80 to $\sim$13 emu/g. A direct calculation indicates that the volume fraction of the FM phase is quite small ($<$5%) at $T = 15$ K (bottom panel in Fig. 1), well below the percolation threshold (20–30 %).[33] This result seems to be in conflict with the conclusion that large polaron diffusion appears only when the system is magnetically saturated. It could be a signature for the presence of threadlike conducting paths, noting the fact that the variation of the FM population affects the electric conductivity but not thermopower when percolation is retained (Refs. 33–35).

The discrepancy of the magnetization and resistivity under the field of 2 T, the latter remains metallic as the former drops, is also consistent with the picture of threadlike conduction. The bottom panel of Fig. 1 shows that the FM frac-

tion is below the percolation threshold at very low temperatures. This implies an insulating conduction, as occurred under the field of 1.5 T. However, different from the case of 1.5 T, the threads can be fully stabilized by the field of 2 T, and a metallic conduction occurs even below the percolation threshold. Whether filamentary conducting paths can be formed in the absence of electric field is still a problem, though short-range order was also observed in $Pr_{0.67}Ca_{0.33}MnO_3$ without applied current (FM phase exists as thin layers in the AFM matrix, forming a red cabbage structure),[36] and further work in this regard is required to get a deep insight into the anomaly in electric and thermopower and/or thermal conductions.

In conclusion, a systematic investigation on the magnetic, electronic, and thermal transport properties of $Eu_{0.55}Sr_{0.45}MnO_3$ has been performed. The compound is found to exhibit a complex magnetic behavior with the change of temperature and magnetic field. Without magnetic field, it stays in a Griffiths-like state in a wide temperature range above $\sim$100 K, characterized by the presence of FM clusters of the size of $\sim$8 Mn ions and an AFM state below $\sim$100 K, evidenced by thermopower and heat conductivity. FM phase emerges and grows in the AFM matrix with applied field, resulting in a series of phase transitions from the PM state first to the AFM state, then to the FM and the AFM states upon cooling ($\sim$0.8 T $< H <$ $\sim$1 T), or a simple PM-FM transition ($H >$ $\sim$2.3 T). The AFM state is unstable under high fields, and the high- and low-temperature AFM transitions are depressed by the fields above 1 and 2.3 T, respectively. The FM transition is incomplete when the field is below $\sim$1.5 T, leading to a coexistence of the FM and PM (or AFM) phases in the intermediate temperature range. A spin-glass-like behavior is observed in the AFM background below $\sim$50 K. Significant response of resistance, thermopower, and heat conduction to magnetic transition, either FM or AFM transition, has been observed. Unlike the typical AFM manganites, for which usually a depression of thermal conduction occurs at the AFM state, the AFM transition at $\sim$100 K in $Eu_{0.55}Sr_{0.45}MnO_3$ enhances the thermal conduction. From the PM phase to the AFM phase and to the FM phase, thermal conductivity increases monotonically. A remarkable result of the present work is the different behaviors of thermopower and resistivity. The former displays the metallic behavior below a distinct temperature that is significantly lower than the metal-to-insulator transition temperature determined by resistivity. Furthermore, thermopower remains metallic while the resistivity shows up an upturn due to the AFM transition in the low-temperature range under the field of 1.5 T. Based on these studies, a magnetic phase diagram is proposed.

*Author to whom correspondence should be addressed; jrsun@g203.iphy.ac.cn

[1] For a review, see *Colossal Magnetoresistance, Charge Ordering, and Related Properties of Manganese Oxides*, edited by C. N. R. Rao and B. Raveau (World Scientific, Singapore, 1998); *Colossal Magnetoresistance Oxides*, edited by Y. Tokura (Gordon and Breach, London, 1999); M. B. Salamon and M. Jaime, Rev. Mod. Phys. **73**, 583 (2001).

[2] C. Zener, Phys. Rev. **82**, 403 (1951).

[3] P. W. Anderson and H. Hasegawa, Phys. Rev. **100**, 675 (1955).

[4] P.-G. De Gennes, Phys. Rev. **118**, 141 (1960).

[5] A. Asamitsu, Y. Tomioka, H. Kuwahara, and Y. Tokura, Nature (London) **388**, 50 (1997).

[6] K. Miyano, T. Tanaka, Y. Tomioka, and Y. Tokura, Phys. Rev. Lett. **78**, 4257 (1997).

[7] M. Itoh, K. Nishi, J. D. Yu, and Y. Inaguma, Phys. Rev. B **55**, 14408 (1997).

[8] A. Sundaresan, A. Maignan, and B. Raveau, Phys. Rev. B **55**, 5596 (1997).

[9] Y. Tadokoro, Y. J. Shan, T. Nakamura, and S. Nakamura, Solid State Ionics **108**, 261 (1998).

[10] G. J. Liu, J. R. Sun, C. M. Xiong, D. J. Wang, Y. W. Xie, H. W. Zhang, T. Y. Zhao, and B. G. Shen, Appl. Phys. Lett. **87**, 182502 (2005).

[11] E. Dagotto, *Nanoscale Phase Separation and Colossal Magnetoresistance* (Springer-Verlag, Berlin, 2003), p. 339; C. N. R. Rao and B. Raveau, *Colossal Magnetoresistance, Charge Ordering, and Related Properties of Manganese Oxides* (World Scientific, Singapore, 1998), p. 219; A. I. Abramovich, O. Y. Gorbenko, A. R. Kaul, L. I. Koroleva, and A. V. Michurin, Phys. Solid State **46**, 1711 (2004).

[12] D. S. Rana, R. Nirmala, and S. K. Malik, Europhys. Lett. **70**, 376 (2005).

[13] R. P. Type, *Thermal Conductivity* (Academic, London, 1969), Vol. 1.

[14] D. K. C. MacDonald, *Thermoelectricity: An Introduction to the Principles* (Wiley, New York, 1962); R. R. Heikes and R. W. Ure, Jr., *Thermoelectricity: Science and Engineering* (Interscience, New York, 1961).

[15] N. F. Mott and E. A. Davis, *Electronic Processes in Noncrystalline Materials* (Clarendon, Oxford, 1979).

[16] K. Knížek, J. Hejtmánek, Z. Jirák, C. Martin, M. Hervieu, B. Raveau, G. André, and F. Bourée, Chem. Mater. **16**, 1104 (2004).

[17] I. O. Troyanchuk, N. V. Samsonenko, N. V. Kasper, H. Szymzak, and A. Nabialek, Phys. Status Solidi A **60**, 195 (1997).

[18] J. A. Mydosh, *Spin Glasses: An Experimental Introduction* (Taylor & Francis, Washington, DC, 1993); J. L. Hemmen and I. Morgenstern, *Heidelberg Colloquium on Spin Glasses* (Springer-Verlag, Berlin, 1983).

[19] K. F. Wang, Y. Wang, L. F. Wang, S. Dong, D. Li, Z. D. Zhang, H. Yu, Q. C. Li, and J.-M. Liu, Phys. Rev. B **73**, 134411 (2006).

[20] Number of the FM cluster will be N/m if m Mn ions form a FM cluster, and the magnetic moment of each FM cluster is $mgS\mu_B$. Replacing N with N/m and S with mS, one obtains the modified Curie-Weiss law, $\chi \approx Nmg^2S^2\mu_B^2/3k_B(T-T_\theta)$ ($mS \gg 1$). According to the derivation of the Curie-Weiss law [C. Kittel, *Introduction to Solid State Physics*, 5th ed. (Wiley, New York, 1976)], whether m is dependent on temperature and/or magnetic field will not affect the above expression.

[21] P. S. Anil Kumar, P. A. Joy, and S. K. Date, J. Phys.: Condens. Matter **10**, L269 (1998).

[22] M. B. Salamon and S. H. Chun, Phys. Rev. B **68**, 014411 (2003); P. Y. Chan, N. Goldenfeld, and M. Salamon, Phys. Rev. Lett. **97**, 137201 (2006).

[23] N. W. Ashcroft and N. D. Mermin, *Solid State Physics* (Thomson Learning, New York, 1976).

[24] M. Jaime, M. B. Salamon, M. Rubinstein, R. E. Treece, J. S. Horwitz, and D. B. Chrisey, Phys. Rev. B **54**, 11914 (1996); H. Sakata, K. Kikuchi, H. H. Qiu, H. Shimizu, and M. Amano, J. Mater. Sci.: Mater. Electron. **10**, 643 (1999); A. Mansingh and A. Dhawan, J. Phys. C **11**, 3439 (1978); S. P. A. Banerjee, E. Rozenberg, and B. K. Chaudhuri, J. Appl. Phys. **89**, 4955 (2001).

[25] W. Archibald, J.-S. Zhou, and J. B. Goodenough, Phys. Rev. B **53**, 14445 (1996).

[26] J. L. Cohn, J. J. Neumeier, C. P. Popoviciu, K. J. McClellan, and Th. Leventouri, Phys. Rev. B **56**, R8495 (1997).

[27] C. Wood, D. Emin, and P. E. Gray, Phys. Rev. B **31**, 6811 (1985).

[28] J. Hejtmanek, Z. Jirák, Z. Arnold, M. Maryško, S. Krupička, C. Martin, and F. Damay, J. Appl. Phys. **83**, 7204 (1998).

[29] K. H. Kim, M. Uehara, C. Hess, P. A. Sharma, and S-W. Cheong, Phys. Rev. Lett. **84**, 2961 (2000).

[30] J. Hejtmanek, Z. Jirák, M. Maryško, C. Martin, A. Maignan, M. Hervieu, and B. Raveau, Phys. Rev. B **60**, 14057 (1999); H. Fujishiro, Physica B **307**, 57 (2001).

[31] A. I. Kurbakov, A. V. Lazuta, V. A. Ryzhov, V. A. Trounov, I. I. Larionov, C. Martin, A. Maignan, and M. Hervieu, Phys. Rev. B **72**, 184432 (2005).

[32] A. I. Abramovich, L. I. Koroleva, A. V. Michurin, O. Yu. Gorbenko, A. R. Kaul, M. Kh. Mashaev, R. Szymczak, and B. Krzhymanska, Phys. Solid State **44**, 927 (2002).

[33] H. Scher and R. Zallen, J. Chem. Phys. **53**, 3759 (1970); S. Kirkpatrick, Rev. Mod. Phys. **45**, 574 (1973); I. Webman, J. Jortner, and M. H. Cohen, Phys. Rev. B **14**, 4737 (1976).

[34] A. Asamitsu, Y. Tomioka, H. Kuwahara, and Y. Tokura, Nature (London) **388**, 50 (1997).

[35] J. Stankiewicz, J. Sesé, J. García, J. Blasco, and C. Rillo, Phys. Rev. B **61**, 11236 (2000).

[36] Ch. Simon, S. Mercone, N. Guiblin, C. Martin, A. Brûlet, and G. André, Phys. Rev. Lett. **89**, 207202 (2002).